Philosophical Magazine A
Publication details, including instructions for authors and subscription information:
http://www.tandfonline.com/loi/tpha20

The cyclic loading of saline ice

David M. Cole [a] & Glenn D. Durell [a]
[a] US Army Cold Regions Research and Engineering Laboratory, Hanover, New Hampshire, USA
Published online: 27 Sep 2006.

PHILOSOPHICAL MAGAZINE A, 1995, VOL. 72, NO. 1, 209–229

The cyclic loading of saline ice

By DAVID M. COLE and GLENN D. DURELL

US Army Cold Regions Research and Engineering Laboratory, Hanover, New Hampshire, USA

[*Received 18 April 1994*† *and accepted 23 December 1994*]

ABSTRACT

This paper details the results of an experimental programme to investigate the constitutive behaviour of saline ice under reversed direct-stress conditions. The test material was laboratory-grown saline (NaCl) ice. The work explored the effects of temperature (from -5 to $-50°C$), cyclic stress amplitude (0·1–0·8 MPa) and loading frequency (10^{-3}–1 Hz) on the response of the ice. Variations in the ice growth conditions allowed the effects of microstructural variations to be investigated as well, with total porosity in the range 30–104 ppt. The experiments were generally performed by applying a sinusoidally varying uniaxial load, oscillating about zero, to the cylindrical specimens. Several experiments employed cyclic strain control. The material response was typically composed of elastic and anelastic strain, with various degrees of permanent or viscous strain occurring at higher temperatures and lower frequencies, and proved to be very sensitive to variations in loading conditions and to microstructural variations. An increase in total porosity caused a decrease in the effective modulus and an increase in the anelastic strain. The ice exhibited a very complex temperature dependence, a stress dependence that was approximately linear at low temperatures and nonlinear at high temperatures, and a significant frequency effect.

§ 1. INTRODUCTION

This paper details observations of the behaviour of laboratory-grown S2 saline ice to reversed direct-stress testing. The experiments employ a patented gripping system that provides an efficient means of systematically examining ice behaviour under alternating tension–compression loading for the first time. The present work concentrates on giving the experimental results and laying the groundwork for the model development presented by Cole (1994, 1995).

In recent years, considerable effort has been directed towards placing our understanding of the mechanical properties of sea ice on a more firm physical basis. To this end, the study of cyclic loading effects in ice serves a twofold purpose. On one level, the experiment directly provides information of practical concern for addressing problems such as the repeated flexure of an ice sheet under vehicular or wave action and thermally induced loading. On a more basic level, the reversed direct-stress experiment provides a sensitive measure of microstructural, thermal, frequency and amplitude effects on the low-strain constitutive behaviour of ice. Such fundamental information on the mechanical properties of this complex material is critical to identifying deformation mechanisms and thus serves as a vehicle for the development of detailed theories of mechanical behaviour.

---

† Received in final form 16 December 1994.

§ 2. Background

Applying forced oscillations to specimens with the reversed direct-stress technique has long been used to examine the inelastic properties of crystalline materials (Mott, 1957, Kressel and Brown 1967, Anglada and Guiu 1981, Biermann *et al.* 1993). This technique allows the examination of temperature, frequency and stress level effects on material response for virtually constant microstructural conditions. Although used for studying cyclic plasticity effects (for example Langdon and Gifkins (1983) and Gabb and Welsch (1989)), it is well suited to the study of high-temperature anelasticity (Nowick and Berry 1972, Gaboriaud Worgard, Gerland and Riviere 1981) where microstructural changes are easily induced in quasistatic experiments. The typical frequency range 10^{-4}–10 Hz is suitable for studying dislocation and grain-boundary relaxation processes.

The creep anelasticity (sometimes referred to as delayed elasticity) of freshwater ice has been examined in compression by Duval (1978), Sinha (1979) and Cole (1991). Anelasticity for nominally constant microstructures has been examined using resonance methods (Kuroiwa 1965), cyclic torsion (Nakamura and Abe 1979, Tatibouet Perez and Vassoille 1985, 1987), repeated loading in compression (Traetteberg, Gold and Frederking 1975) and the reversed direct-stress method (Cole 1990a, 1993, 1994). Cyclic compressive loads, of a sufficient magnitude to produce flow with microcracking, have also been applied to saline ice (Tabata and Nohguchi 1979) and freshwater ice (Mellor and Cole 1981).

Early indications of grain size effects in ice prompted explanations of anelasticity based solely on grain-boundary sliding (Sinha 1979), while others (Vassoille, Mai and Perez (1978) testing single crystals, and Duval (1978) testing polycrystals) viewed the process essentially as a high-temperature dislocation background. Cyclic torsional experiments on freshwater ice (Tatibouet *et al.* 1987) showed a distinct grain-boundary relaxation peak and a background that increased with increasing basal dislocation density. Since non-basal contributions to macroscopic slip are minimal (Higashi 1966, Shearwood and Whitworth 1989) in ice Ih (the hexagonal form that exists under environmental conditions), dislocation-based anelasticity is generally attributed to the motion of (0001) $\langle 11\bar{2}0\rangle$ dislocations.

Although sea ice exhibits a large anelastic relaxation (for example Tabata (1958), Vaudrey (1977) and Gladkov *et al.* (1983)), systematic studies have only recently been initiated (Cole and Gould 1989, Cole 1990b). Alternately applying zero-mean-stress cyclic loads and compressive creep loads, Cole (1993) demonstrated that the anelasticity of laboratory-grown saline ice increases dramatically with increasing accumulated creep strain and that the effect was strongest during primary creep. These findings echo those of Tatibouet *et al* (1987) on fresh-water ice and demonstrate that, despite dissimilar microstructures, similar dislocation-based processes operate in both saline and fresh-water ice.

Ice undergoes a mechanical relaxation from the stress-induced ordering of protons (Onsager and Runnels 1969) in kilohertz range, and a dislocation resonance peak has also been found in the megahertz range (Hiki and Tamura 1983). However, since both mechanisms are very weak ($\tan \phi_{\max} = 9 \times 10^{-3}$ and 4×10^{-4} respectively), they are ignored in the present work.

It thus appears that, for practical considerations, sea-ice anelasticity can be largely understood through the combined effects of grain-boundary and basal dislocation contributions and the influence of microstructure on the extent to which these mechanisms can operate. There is need to quantify these mechanisms fully since sufficient confusion exists, especially regarding microstructural effects, that even the most recent efforts (Zhan, Evgin and Sinha 1994) resort to empiricism when modelling ice anelasticity. The present study was conducted to provide an improved physical understanding of these relaxation processes and to elucidate the role of microstructure.

§ 3. Experimental details

Most experiments were performed in load control, but several were performed in strain control, on a closed-loop electrohydraulic testing system. In either mode, the command signal was a zero-mean-stress sinusoid. A load cell mounted in line with the specimen monitored the axial load, and two displacement transducers mounted on circumferential rings at third points along the length of the specimen provided the deformation measurements. Digitized records provided 200 points per load cycle regardless of frequency.

The raw data are smoothed using procedures described by Cole and Durell (1995), and quantities of interest (stress–strain curves, initial moduli $\partial\sigma/\partial\varepsilon|_{\sigma=0}$, hysteresis loop width (along $\sigma = 0$) and area, and internal friction) are calculated from these smoothed points. Cole and Durell (1995) also details the patented system employed for attaching the ice specimens to the testing machine without imposing stress concentrations or a bending moment during either clamping or subsequent load application. This hydraulically activated device overcomes the difficulties of rigidly mounting large-diameter specimens (up to 100 mm) of a low-fracture-strength material with a unique ball and race configuration for self-alignment. The rigid end conditions have been shown by G'Sell and Champier (1981) to result in an optimally uniform stress field.

Most of the specimens were obtained from laboratory-grown blocks of saline (NaCl) ice. A range in physical properties of the specimens was achieved by varying the initial meltwater salinity from 3·5 to 34 ppt. Heat was extracted from the top surface by a cold plate. Once the block reached the desired thickness, it was removed from the tank and placed in a -10°C coldroom overnight. A block typically remained at -10°C for 1–3 days before cores were obtained. The coring operation produced very well finished right circular cylinders with a diameter of approximately 102 mm and length of approximately 0·3 m. Immediately prior to an experiment, specimens were trimmed and given end caps following proceedings described by Cole, Gould and Burch (1985).

Specimens that were not tested immediately after coring and trimming were tightly wrapped and stored at -30°C. Either after coring or upon removal from deep storage, specimens were allowed to equilibrate overnight in the circulating air environmental chamber at the benchmark test temperature of $-10 \pm 0{\cdot}2$°C. To provide a basis for comparison, every specimen was examined initially at this temperature. Specimens tested over a range of temperatures had consistent thermal histories and details have appeared in the report by Cole and Durell (1995).

It should be noted that time–temperature effects present an inherent problem in experiments on saline ice owing to the instability of the microstructure at environmental temperatures (Cox and Weeks 1986), and a complete understanding of the governing processes is not yet on hand. Sea ice grows dendritically with a characteristic skeletal layer of forming platelets at the bottom of the sheet. Brine drains from this layer and from communicating voids through the thickness of the sheet when it is removed from the melt, and microstructural changes eventually occur. These processes are unavoidable in isothermal laboratory experiments on this material. The specimens examined herein may have thus experience changes in the size and spatial distribution of the brine-filled inclusions, especially for the very-high-temperature experiments, and the reported physical properties apply to their condition at the end of testing.

Field experiments are the best, if not the only, way to avoid brine drainage effects and the present author is currently engaged in an *in situ* loading programme to validate models based on the laboratory results.

§ 4. Microstructure

Figure 1 illustrates the complex microstructure of the experimental material. The sections run perpendicular to the growth direction and thus cut the columnar grains along their short dimension. The range of magnifications allows assessment of the microstructural features from the scale of the grains (about 5–15 mm) to that of the inclusions (about 0·1 mm). As the dendrites thicken during freezing to form the relatively pore-free regions evident in fig. 1, brine- and gas-filled voids congregate along well defined planes (platelet boundaries) to form the characteristic sea-ice microstructure. The brine inclusions tend to be elongated in the growth direction and there are vast differences in their shapes, sizes and interconnectedness.

As a consequence of growth under quiescent laboratory conditions, the c axes of the columnar crystals are confined to lie approximately in the plane of the sheet and are randomly oriented (unaligned) in that plane (Weeks and Ackley 1982). The coring direction and therefore the axis of applied stress for the specimens examined were orthogonal to the growth direction.

Table 1 gives the physical properties of the specimens along with the salinity of the tanks prior to the start of freezing. The porosity calculations are based on the equations presented by Cox and Weeks (1983) and the methods of grain size determinations are indicated.

§ 5. Experimental results

5.1. *General characteristics of the cyclic loading response*

Figure 2 shows a typical hysteresis loops (specimen HOP2; $T = -30°C$; $\sigma = \pm 0{\cdot}6$ MPa) for frequencies of 1, 10^{-1}, 10^{-2} and 10^{-3} Hz. The extent to which viscous straining occurred during any half-cycle can be determined from the difference between the initial strain and the strain after unloading and full recovery. Specimen rebound after unloading was monitored until no change could be detected by the measuring system. The required times were approximately equal to one period of loading. There is very little permanent straining associated with the loop at 10^{-3} Hz (about 11% of the total loop width) and none at the higher frequencies at the prevailing temperature; so the observed losses are predominantly anelastic. A detectable anelastic strain exits at 1 Hz and $-30°C$, amounting to about 13% of the peak elastic strain. The hysteresis loops in fig. 2 illustrate the strong frequency dependence of the anelastic loss and the transient behaviour as the anelastic process becomes fully engaged during the first cycle.

Under load control, the peak strain in the first cycle can exceed the steady-state strains and, in strain control, the peak stress during the first cycle is lower than in subsequent cycles. The material generally reaches a nominal steady state after the first cycle, although a tendency in load control for the loops to migrate slowly towards compressive strains when the loading begins in tension, and towards tensile strains with initial loading in compression, is frequently evident.

Fig. 1

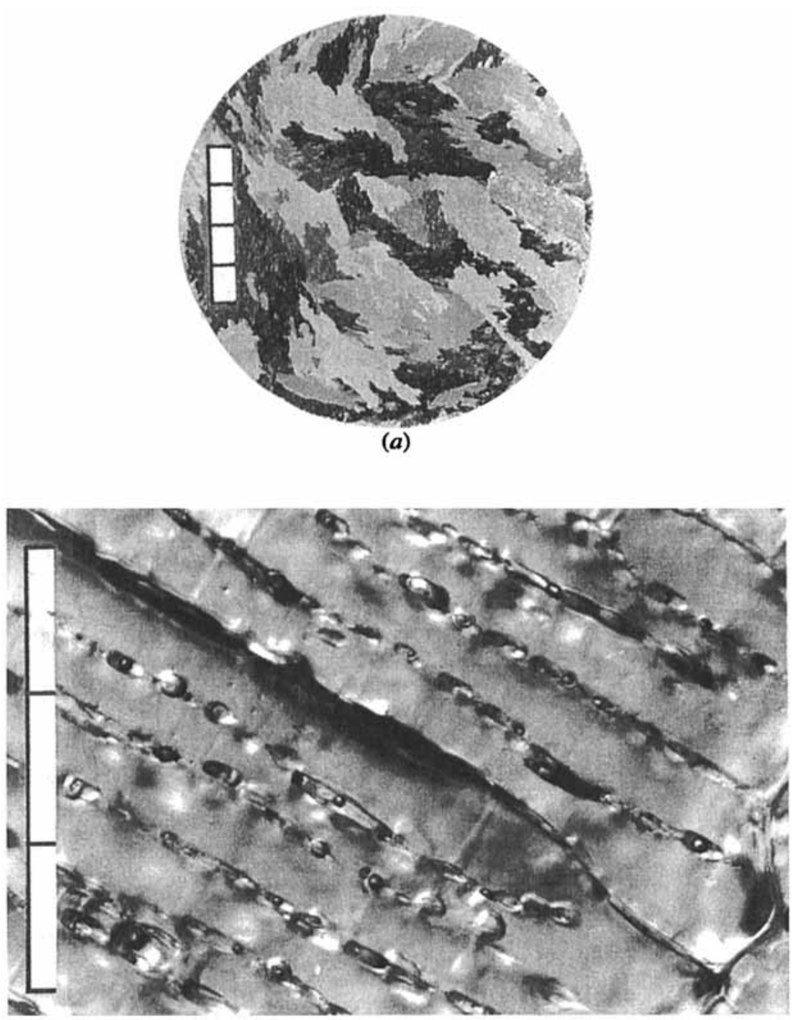

(*a*)

(*b*)

Thin section of experimental material: (*a*) specimen DY1V1, viewed in the growth direction under cross-polarized light, with a scale division of 10 mm: (*b*) micrograph of specimen DC1-1 viewed in the growth direction under transmitted light, with a scale division of 1 mm.

Table 1. Physical properties of specimens: (a), grain size determined from average grain area; (i), grain size determined by linear intercept method.

Specimen	Tank salinity (‰)	Specimen salinity (‰)	Density ($Mg\,m^{-3}$)	Porosities measured at −15°C Brine	Gas	Total	Grain size (mm)	Platelet spacing (mm)
HOF1	7	2·4	0·902	0·0096	0·0212	0·0308	10 (a)	0·5
HOF2	7	2·6	0·886	0·0103	0·0387	0·0490	5·4 (i)	–
DY1V1	15	4·1	0·893	0·0163	0·0327	0·0490	12·1 (i)	0·6
DY1H1	15	4·4	0·934	0·0183	–	–	6·1 (a)	0·4
NP5-1	15	6·6	0·878	0·0258	0·0515	0·0774	10·1 (a)	0·5
NP5-3	15	7·0	0·89	0·0278	0·0390	0·0667	11·2 (a)	0·5
PL24C	24	2·3	0·881	0·0090	0·0438	0·0529	11·1 (a)	0·5
DC-1	34	10·4	0·87	0·0403	0·0640	0·1044	8·7 (a)	0·3
DC1-2	34	10·6	0·9	0·0425	0·0320	0·0745	6 (a)	0·4
DC1-3	34	9·5	0·882	0·0374	0·0502	0·0876	15·5 (a)	0·5
DC2-1	34	5	0·862	0·0192	0·0672	0·0864	8·5 (a)	0·5
DY2H2	15	4·4	0·878	0·0172	0·0493	0·0665	5·9 (a)	0·3
DY2H3	15	4	0·859	0·0153	0·0694	0·0847	4·8 (i)	–
DY2H4	15	5·8	0·878	0·0227	0·0507	0·0734	8·3 (a)	0·4
DY4H1	15·5	4·5	0·913	0·0183	0·0115	0·0298	6·1 (i)	–
DY4H2	15·5	4·3	0·91	0·0174	0·0145	0·0319	9·7 (a)	–
DY4H3†	15·5	4·5	0·912	0·0179	0·0130	0·0309	4·1 (i)	–
DY5H1†	8	6·8	0·903	0·0272	0·0247	0·0519	4·4 (i)	–
DY7H1†	8	2·8	0·892	0·0108	0·0326	0·0434	6·8 (a)	–
HOP2†	3·5	0·1	0·884	0·0004	0·0383	0·0387	–	–
HOP3	3·5	0·1	0·884	0·0004	0·0383	0·0387	3·2 (i)	–
HOJ4	7	3	0·892	0·0119	0·0326	0·0446	9·5 (a)	–

† Properties taken from adjacent material.

Fig. 2

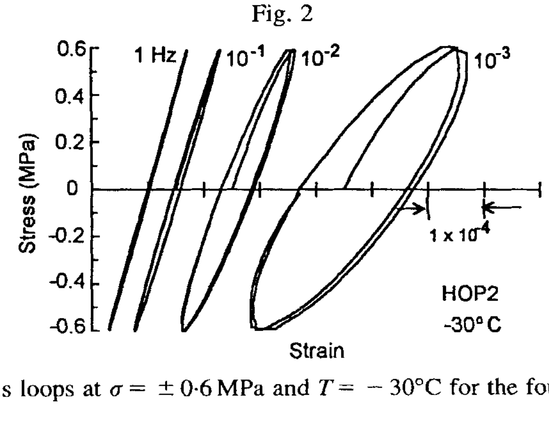

Typical hysteresis loops at $\sigma = \pm 0{\cdot}6$ MPa and $T = -30°C$ for the four test frequencies.

Fig. 3

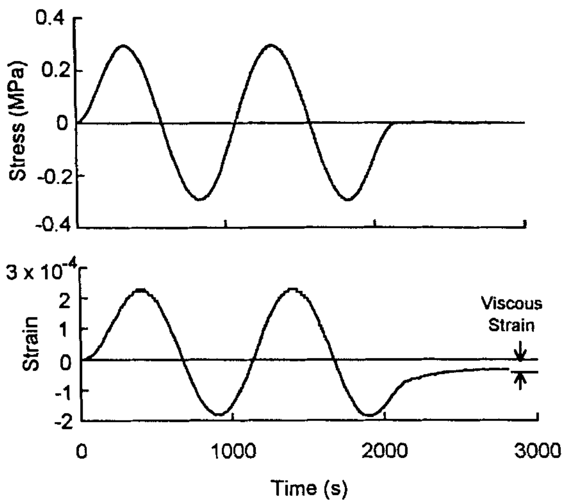

Stress and strain against time, illustrating the determination of the viscous strain contribution (specimen DY5H1; $T = -10°C$; 10^{-3} Hz).

Fig. 4

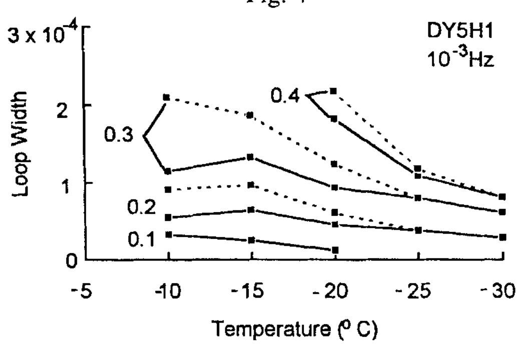

Loop width against temperature for a frequency of 10^{-3} Hz and stress levels as indicated: (- - - -), full loop widths; (———), estimated anelastic component after subtraction of the viscous strain.

5.2. *Viscous straining*

Experiments at high temperatures and low frequencies resulted in the accumulation of viscous strain during load cycles, manifested as an offset between the final and initial strains (fig. 3). Given the focus of the present work on ice anelasticity, it is important to remove this contribution to the hysteresis loop widths. Figure 4 shows the results of subtracting the viscous strain estimates from the total loop widths. (broken lines) to produce an estimate of the anelastic strains (solid lines). Viscous strain composed up to about 30% of the total loop width for 10^{-3} Hz and up to 20% at 10^{-2} Hz for temperatures above $-10°C$. Additionally, for the range of applied stresses at 10^{-3} Hz, there was no discernible creep deformation at temperatures of $-40°C$ and below, and total contributions of less than 10% could be measured at $-30°C$.

Fig. 5

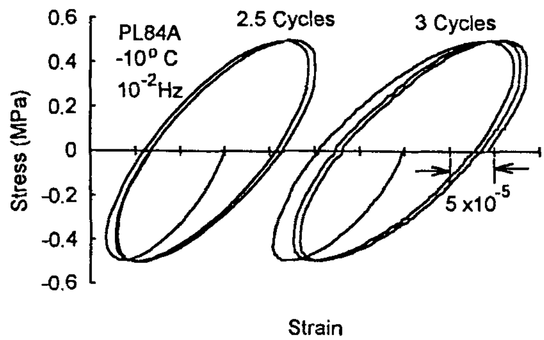

Hysteresis loops for specimen PL84A, with initial loading in compression, for experimental conditions as indicated, under a nominal cyclic stress of ± 0·5 MPa. The figure shows results for 2·5 cycles and 3 cycles.

Table 2. Anelastic and viscous strain observations after 2·5 and 3·0 cycles for a frequency of 10^{-2} Hz at $T = -10$°C.

Stress (MPa)	Number of cycles	Strain (× 10^5)	
		Viscous	Anelastic
± 0·3	2·5	2·727	5·455
	3·0	3·864	4·773
± 0·5	2·5	8·182	10·0
	3·0	9·318	9·091

5.3. *Tension–compression asymmetry*

The loops generally did not become centred about the initial $\varepsilon = 0$ point by the end of the 2 or 3 cycles that were applied for a given set of conditions. When loaded in tension first, approximately 65% of the loop width consists of tensile strain. Decomposing the loop widths into anelastic and viscous strains indicated that the tensile half cycle systematically produced more viscous strain than the compressive half-cycle. For the steady-state behaviour in load control, the tensile and compressive loop areas are approximately equal. Strain control produced a peak tensile stress that exceeded the peak compressive stress, resulting in a somewhat greater loop area for the tensile half of the cycle.

Several experiments were carried out beginning in compression to ascertain whether the bias towards tensile strain was associated with transient effects or with a more fundamental tension–compression asymmetry in the dislocation behaviour (fig. 5). The overshoot occurs in the direction of initial loading and the loops are shifted towards compressive strains, indicating that these effects are associated with the transient behaviour and not with the polarity of the applied stress.

To gain insight regarding the asymmetry of the viscous response, this specimen was also subjected to 2·5 and 3 cycles of compression-first loading (see fig. 5). The viscous strain corresponds to the difference between the initial strain ($\varepsilon = 0$) and the final strain after full recovery. The anelastic strains given in table 2 correspond to the total loop width minus the viscous strain experienced during the cycle.

Fig. 6

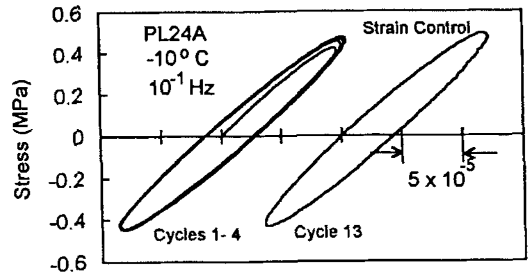

Results of cyclic loading performed on specimen PL24A in strain control.

The anelastic strain shows a 10–14% bias favouring the direction of initial loading, but the tensile viscous strains exceed the compressive viscous strains by an average of 28% regardless of the direction of initial loading. Since full cycles (beginning in tension) were applied in most of the experiments, only the viscous strain for the compressive half-cycles is available. Therefore, when viscous straining was observed, its total contribution to the loop width was estimated by multiplying the compressive half-cycle value by a factor of 2·28 to account empirically for the tension–compression asymmetry. There are insufficient observations for a detailed consideration of this matter at the present time and additional experiments of this type are currently in progress.

5.4. *Strain-controlled experiments*

Figure 6 shows the first to fourth cycles and the thirteenth cycle of a specimen subjected to cyclic strain control at a frequency of 10^{-1} Hz. The strain amplitude was approximately $\pm 4{\cdot}6 \times 10^{-5}$, which resulted in an average stress amplitude of $\pm$ 0·46 MPa, and transient effects are primarily evident in the first cycle. The shape of the steady-state hysteresis loops was essentially the same as obtained in load control. The peak tensile and compressive stresses are + 0·495 and − 0·43 MPa respectively, and the loop area above the strain axis ($\sigma = 0$) is approximately 16% greater than the area below the axis. These observations indicate that the phenomenon responsible for the slight shift to positive strains in load control produces a shift to positive stresses in strain control.

5.5. *Effect of number of cycles*

To examine the effect of continuous cycling near the tensile strength of the ice, an initial applied stress of approximately $\pm$ 0·5 MPa was incremented by 0·1 MPa every 50 cycles until tensile failure occurred. This load history had virtually no effect on the cyclic loading response. The hysteresis loops essentially retained their shape throughout the experiments and no systematic change in loop area with continued cycles was evident. The initial modulus did not vary systematically with accumulated cycles or stress level. Energy loss per cycle increased with increasing stress as expected but showed no systematic variation with accumulated cycles at any given stress level. Tensile failure usually occurred upon the first application of a critical stress level, but several failures took place after several cycles of a critical stress. The absence of hardening (or softening) effects during continuous cycling indicates that significant

Fig. 7

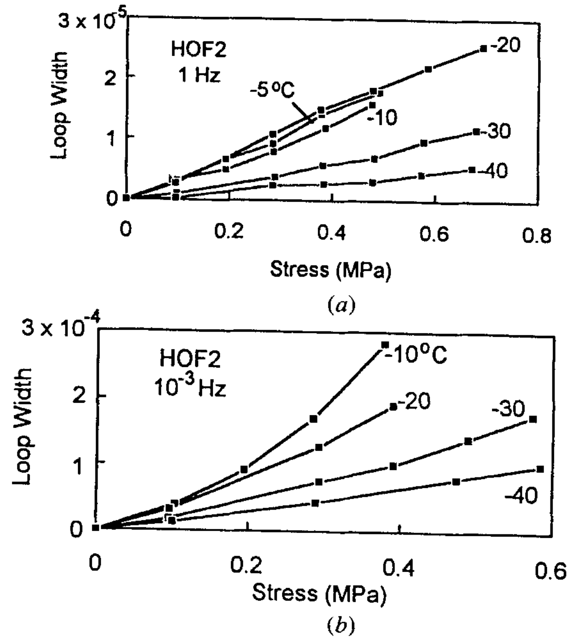

Loop width against peak cyclic stress for specimen HOF2 for various temperatures and frequencies of (*a*) 1 Hz and (*b*) 10^{-3} Hz.

microstructural changes such as the formation of complex dislocation substructures do not occur for the present range of conditions.

5.6. *Stress dependence of anelastic strain*

The peak cyclic stresses ranged from $\pm 0{\cdot}1$ to $\pm 0{\cdot}8$ MPa, in increments of 0·1 or 0·2 MPa. Figure 7 show the stress dependence of the anelastic strain for the frequencies and temperatures indicated. The 1 Hz results are linear at all temperatures, whereas nonlinear behaviour emerges at 10^{-3} Hz at higher temperatures. The intermediate frequencies produce responses that transition between these two cases. A specimen with a relatively high tensile strength (PL85C) showed evidence of a transition to nonlinear behaviour above approximately $\pm 0{\cdot}6$ MPa at 10^{-1} Hz and -10°C.

5.7. *Temperature effects on the anelastic straining*

Figure 8 gives the loop widths for specimen HOF2 as a function of temperature for the conditions indicated. The peak that is evident between -10 and -20°C in the 1 Hz results shown in fig. 8 (*a*) is examined below. Figure 9 shows the apparent activation energy Q_a, calculated from a frequency shift analysis of the anelastic strain normalized to the peak stress level. The bars in fig. 9 correspond to the temperature intervals over which Q_a values were determined. A least-squares analysis was employed to calculate Q_a from (Nowick and Berry 1972):

$$\ln\left(\frac{\omega_2}{\omega_1}\right) = \frac{Q_a}{k}(T_1^{-1} - T_2^{-1}), \tag{1}$$

where the subscripts 1 and 2 refer respectively to the -10°C master curve and the data curve being analysed. For the range in experimental conditions, there were no stress

Fig. 8

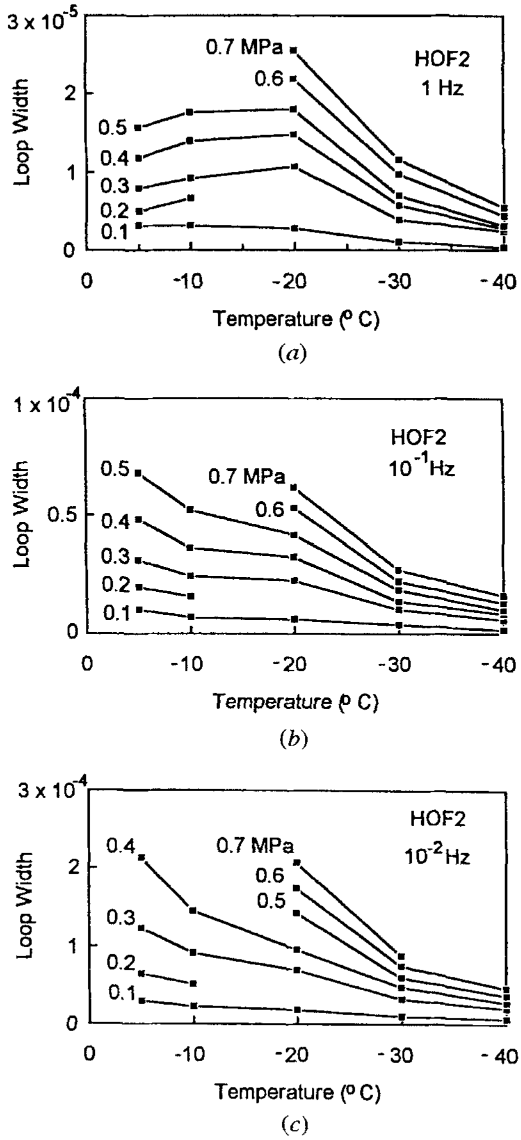

Loop width against temperature for specimen HOF2 for stress levels as indicated: (*a*) 1 Hz; (*b*) 10^{-1} Hz; (*c*) 10^{-2} Hz.

level effects on Q_a and apart from the results at 1 Hz discussed below, Q_a was independent of frequency. The normalized loop width is associated with the loss compliance D_2^d and the master curve was generated by the equation

$$D_2^d = \alpha \delta D^d \frac{1}{\exp(\alpha s) + \exp(-\alpha s)}, \tag{2}$$

where α is a parameter that controls the width of the relaxation peak, δD^d is the total compliance change associated with the mechanism and $s = \ln(\tau_m \omega)$. In the latter

Fig. 9

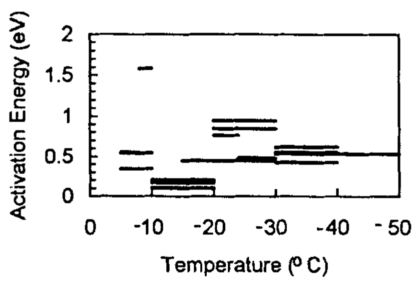

Average activation energy for the anelastic strain calculated from frequency shift, for specimens HOP2, HOF1, HOF2 and PL19. Each bar covers the temperature range over which the calculation was made.

expression, τ_m is the central relaxation time and ω is the angular frequency. Equation (2) produces a Debye relaxation peak when $\alpha = 1$ and broadens with constant area as α decreases. A least-squares analysis of all data gave a value of $\alpha = 0{\cdot}54$. The origin and implications of eqn. (2) have been discussed fully by Cole (1995). This is a well documented approach to address empirically the effects of a relaxation time distribution (Nowick and Berry 1972, Lakki, Schaller, Nauer and Carry 1993). Approximate values of δD^d varied from about 10^{-9} to about $1{\cdot}7 \times 10^{-9}\,\mathrm{Pa}^{-1}$ for the five specimens included

Fig. 10

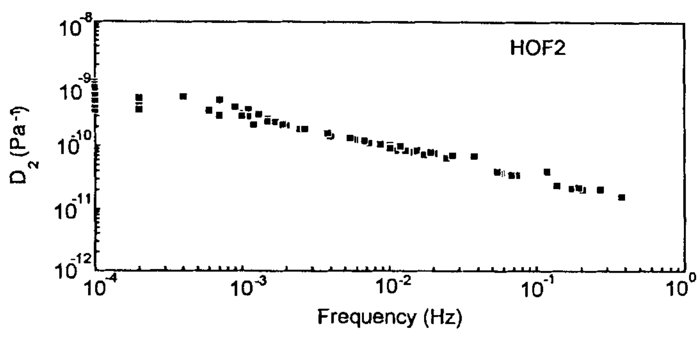

A log–log plot of the loss compliance against frequency for specimen HOF2. Data points have been shifted to a − 10°C master curve.

Fig. 11

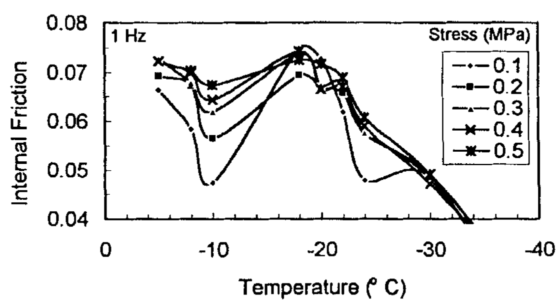

Typical grain-boundary internal-friction peak observed in the 1 Hz results for specimen HOF2.

in the analysis. Figure 10 plots the natural logarithm of the loss compliance against the natural logarithm of the shifted frequency for specimen HOF2. An exponentially increasing background would plot on a straight line in fig. 10, and the observation that the data points fall below the line at low frequencies has implications that are examined in the next section.

Figure 11 shows a typical internal-friction peak found in the 1 Hz results. The magnitude, temperature and frequency associated with this peak correspond to a grain-boundary peak identified by Tatibouet *et al.* (1987). For the data in fig. 12, the maximum in the grain-boundary internal friction curve is $\phi^{gb}_{max} = 7{\cdot}3 \times 10^{-2} \pm 2{\cdot}2 \times 10^{-3}$. The average of all observations is $8{\cdot}8 \times 10^{-2} \pm 1{\cdot}9 \times 10^{-3}$, which agrees with the findings of Tatibouet *et al.* (1987) (about 0·08–0·09) for granular freshwater ice and those of Cole (1994) (0·07–0·085) for granular and columnar freshwater and saline ice specimens.

The use of the word apparent with reference to the activation energy must be stressed in the present context since temperature affects both the extent to which deformation mechanisms can operate and the specimen's microstructure (via the brine porosity). Several observations may be made on the basis of the temperature dependence of the loop width.

(1) The magnitude of Q_a was highly variable at temperatures above approximately -10°C, with average values as high as about 1·58 eV.
(2) Between -10 and -20°C, the anelastic strain was a relatively weak function

Fig. 12

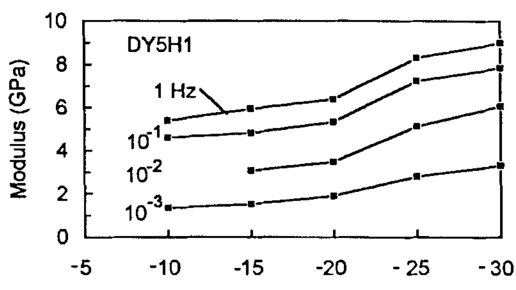

(*a*)

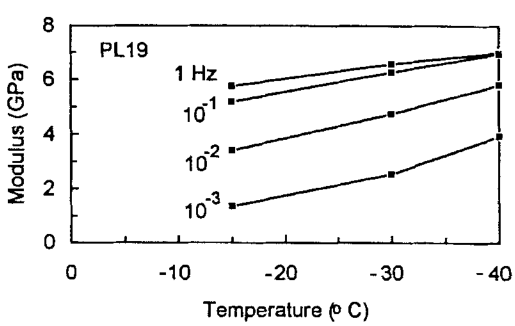

(*b*)

Modulus against temperature for the indicated frequencies: (*a*) specimen DY5H1; (*b*) specimen PL19. The moduli are averages for the initial tensile loading of the second and third cycles.

of temperature, with values of Q_a below about 0·3 eV. A broad relaxation peak occurred at 1 Hz in this temperature range that was accompanied by a dispersion in the modulus. This corresponded to a grain-boundary internal-friction peak with $\phi_{max}^{gb} \approx 0{\cdot}09$.

(3) Depending on the microstructural characteristics of the specimen in a way that is not well understood at this time, the cyclic loading response may change abruptly in the vicinity of the eutectic point. Figure 12 (*a*) shows initial modulus against temperature for specimen DY5H1, tested relatively soon after solidification. In this plot, the abrupt increase in the apparent elastic stiffness occurring between − 20 and − 25°C (which was not consistently reflected in the anelastic strain observations) is believed to be associated with solidification of brine below the eutectic point (− 21·2°C). The older ice examined (specimen PL19 in fig. 12 (*b*)), with its considerably lower salinity, exhibited no abrupt change in either the initial modulus or the loop width.

(4) From approximately − 25 to − 50°C, the average Q_a is about $0{\cdot}52 \pm 0{\cdot}10$ eV, and the scatter in the observations is considerably less than at the higher temperatures. The temperature dependence of the cyclic loading response in this range gives a clearer picture of the underlying dislocation processes because the observations are not influenced by the temperature effects on porosity that occur above the eutectic point.

5.8. *Temperature and frequency effects on the initial modulus*

Figure 13 illustrates the effects of temperature and frequency on the initial modulus. The tensile loading portion of the first cycle generally exhibited a steeper slope than did subsequent cycles, but the temperature dependence was in general very similar to that observed in subsequent loading cycles. The points in fig. 14 are averages for the second and third cycles of loading taken over all applied stress levels (the modulus was found to be independent of the peak stress).

Figure 14 (*a*) gives the average (of the second and third cycles) moduli for specimen HOF2 as a function of frequency for several temperatures. For − 10°C and higher, there appeared a consistent tendency for the slope of the modulus against frequency lines to decrease at the low frequencies. This indication that a lower asymptote might appear reflects the low-frequency trends noted in fig. 10 and prompted the lower-frequency experiments seen in fig. 14 (*b*). This attempt to isolate the anelastic response from viscous strain effects by testing at − 30°C was partially successful. Figure 14 (*b*) gives a good indication that the modulus is continuing its asymptotic approach towards a non-zero value (about 2 GPa), indicating that the lower limit of a relaxation process is being reached. Although the loop widths should exhibit a corresponding trend, it is much less in evidence as a result of uncertainties related to the approximation of the viscous strain contributions discussed earlier.

Figure 15 presents a comparison between the first cycle moduli of saline ice and the observations of Traetteberg *et al.* (1975) for freshwater columnar ice, which typically has the higher modulus of the two materials. The approximate strain rates for the present data were determined by dividing the total strain at the peak (quarter-cycle) by the elapsed time. Both sets of results exhibit degrees of scatter that are typical of first-cycle loading behaviour and which make it difficult to observe whether a low-frequency asymptote exists.

Fig. 13

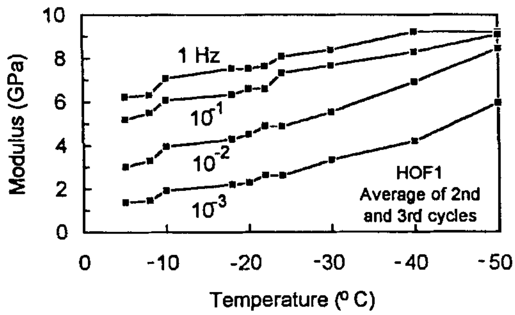

Initial modulus against temperature for specimen HOF1. Data points are averages of second and third cycle values for stress levels of ± 0·2, 0·3 and 0·4 MPa; frequencies are as indicated.

Fig. 14

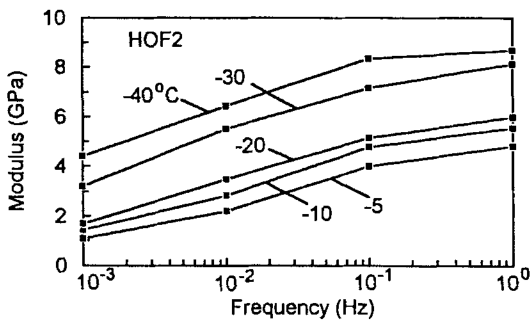

(*a*)

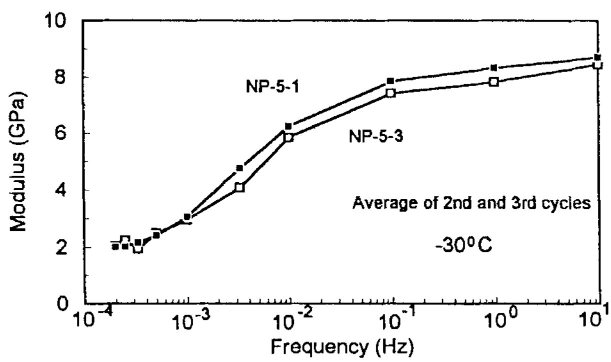

(*b*)

Modulus against frequency for several specimens and temperatures as indicated: (*a*) specimen HOF2; (*b*) specimens NP-5-1 and NP-5-3.

Fig. 15

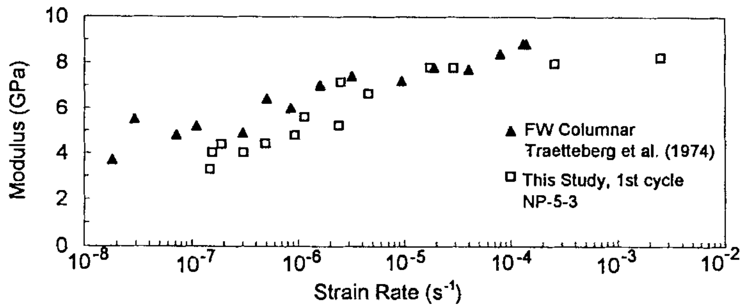

Modulus against strain rate for first-cycle data from specimen NP-5-3 and freshwater (FW) columnar ice values from Traetteberg *et al.* (1975) for comparison. Strain rates were estimated for NP-5-3 from the peak strain divided by a quarter of the period.

Fig. 16

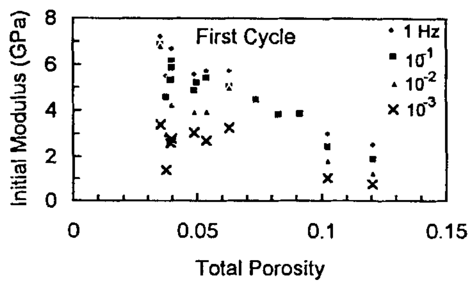

(*a*)

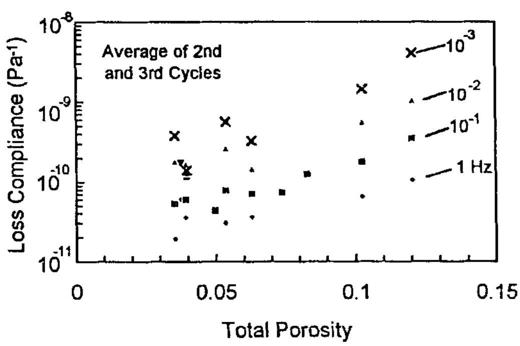

(*b*)

Porosity effects in the initial modulus and loss compliance of all specimens, where the frequencies are as indicated: (*a*) average first cycle moduli; (*b*) average loss compliance for the second and third cycles.

5.9. *Microstructural effects*

Figure 16 illustrates the strong effect that total porosity exerts on the modulus, which is in keeping with earlier findings (for example Vaudrey (1977)). The porosities are calculated for the test temperature of $-10°C$ using the equations presented by Cox and Weeks (1983). Moduli for the second and third cycles behaved similarly. An increase in total porosity from 14·5 to 104·4 ppt caused a 60–70% decrease in the modulus at $-10°C$. The anelastic contribution to straining, as indicated by the loss compliance, also increased by a factor of six to nine, depending on frequency, as seen in fig. 16 (*b*).

Saline ice has long been recognized as more compliant and weaker than freshwater ice by virtually any measure of strength. McKittrich and Brown (1993), for example, in comparing the deformaiton behaviour of freshwater and saline single crystals, found saline ice to deform plastically under conditions that induced significant microcracking in freshwater single crystals. Experimental evidence and associated models indicate that dislocations can be generated in directionally solidified materials when the thermal gradient generates sufficiently high shear stress to generate dislocations (Tsai, Yao and Chait 1992). although this process may contribute, the observation that pore-free freshwater ice grown in the same thermal regime as the present saline specimens typically exhibits a significantly lower dislocation-based compliance (Cole 1994, and unpublished results) indicates that other mechanisms, perhaps peculiar to saline ice, may be involved. Freezing strains from the cooling of brine-filled inclusions are expected to generate dislocations in saline ice (Gupta, Picu and Frost 1993) in much the same manner as in metal matrix composites (Dunand and Mortensen 1991). The observation of slight misorientations between adjacent platelets could be relevant in so far as grown-in dislocations are concerned. The lateral growth and eventual joining of dendrites could result in higher dislocation densities because of the requirement for misfit dislocations to accommodate misorientations between adjacent platelets. More experiments of a fundamental nature are needed to clarify this matter.

No systematic variations between the cyclic loading response and grain size, which varied from 3·2 to 15·5 mm, emerged when specimens of similar porosities were compared. However, this might be expected on the basis of Cole's (1994) work, where it was found that the effective modulus of granular freshwater ice was effectively independent of grain size for $d > 3$ mm.

§ 6. Discussion

Examining dislocation-based anelastic relaxation in ice presents a quandary since the lower test temperatures needed to inhibit viscous effects shift the relaxation peak, requiring lower experimental frequencies, which in turn promote viscous straining. Consequently, it may not be physically possible to capture fully a dislocation relaxation peak for ice that is completely unaffected by viscous effects. Despite this, there is reasonable indication, especially in the modulus behaviour at low frequencies, that a low-frequency asymptote exists for saline ice. although fundamentally a manifestation of the same process underlying creep anelasticity, it must be emphasized that the present results apply to a constant and not evolving microstructure.

Interestingly, the value of $\phi_{max}^{gb} = 0{\cdot}09$ for saline ice is consistent with values observed for identifiable grain-boundary sliding in other materials, typically less than 0·1 (for example Shigenaka, Manzen and Mari (1993) and Zhu and Kê (1989)). Although the process of grain-boundary sliding has been invoked to explain ice anelasticity (Sinha 1979, 1990), this relatively weak mechanism cannot alone explain the magnitude or relaxation time characteristics of saline ice anelasticity. The simultaneous operation of distinct dislocation and grain-boundary relaxation processes, however, can explain the relaxation strength and observations (Traetterberg *et al.* 1975, Gold 1994) that a relaxation time of about 1 s (owing to grain boundaries) characterizes the initial recovery of polycrystalline specimens, with subsequent relaxation (due to dislocations) characterized by increasingly longer relaxation times. The magnitude of the dislocation relaxation peak ($\phi^{d}_{max} \approx 0{\cdot}35$–$0{\cdot}40$), while comparable with high-temperature background observations (for example Lakki, Schaller, Nauer and Carry (1993) who tested yttria-doped zirconia polycrystals) is very large compared with values in the range $\phi_{max} = 0{\cdot}04$–$0{\cdot}06$ that are typical for high-temperature dislocation peaks found in copper and copper–aluminium solid solutions (for example Gaboriaud *et al.* (1981)). Internal friction maxima comparable with the present values have been observed; Woirgard, Riviere and De Fouquet (1981) reported dislocation internal-friction peak heights from 0·15 to 0·7 in aluminium single crystals. The frequency range for these dislocation peaks generally coincides with that of the present work. As noted by Woirgard *et al.* (1981), and further discussed by Cole (1995), the fact that the relaxation is so large directly affects the choice of physically admissible models.

Although not the focus of the present effort, the tension–compression asymmetry found in the early stages of viscous straining has potentially important implications. Similar behaviour has been attributed to asymmetric behaviour of screw dislocations under reversed stress (Bowman and Gibala 1992), to normal stress effects on the dislocation core (Takasugi *et al.* 1993), to twinning–antitwinning asymmetry or the operation of different slip systems upon stress reversal (Chang, Taylor and Christian 1983), and to stress field effects on the operative deformation mechanisms (for example void growth in tension only (Wiederhorn *et al.* 1988)). The latter alternative holds particular promise since Higashi (1966) observed void formation during tensile creep involving non-basal glide in fresh-water ice single crystals at stress levels comparable with those in the present work. The present author has observed similar creep asymmetry in freshwater ice as well, and current experiments address this matter with both cyclic and constant-load experiments.

Temperature affects the observed straining through its influence on the lattice constants, on total porosity and on the operative inelastic deformation mechanisms. The present results for NaCl ice may be expected to exhibit a simpler temperature dependence than standard sea ice, which contains several additional salts that precipitate at different temperatures (Assur 1958). Although somewhat low, the present range of Q_a for temperatures below the eutectic point is in fair agreement with the values near 0·6 eV for the glide of basal dislocations of mixed character found by Mai (1976) and Fukuda, Hondoh and Higashi (1987). Data reported by Cole (1995) indicate a value of 0·54 eV for single crystals of pure ice under reversed direct-stress cyclic loading. For reference, the activation energy for viscous straining in freshwater polycrystalline ice is 0·7 eV (Hobbs 1974). It is noted that Shearwood and Whitworth (1991) reported activation energies near 0·9 eV for individual dislocations of well defined character, but these significantly higher values have not yet been reconciled with the observed behaviour of large groups of dislocations.

§ 7. Conclusions

From the results obtained in this study on the response of saline ice to cyclic loading, and given the experimental conditions and limitations detailed in the foregoing text, the following conclusions are drawn.

(1) The reversed direct-stress testing method is well suited to the examination of the constitutive behaviour of saline ice at low strains and for stresses below the tensile failure stress.
(2) The temperature dependence of the effective elastic and anelastic response is complex, with several regimes of behaviour characterized by significant changes in the apparent activation energy. Material tested relatively soon after growth exhibited a significant increase in the effective elastic modulus and decrease in loss compliance as temperature dropped below the eutectic point. Older ice did not exhibit significant changes in properties relative to the eutectic.
(3) The material exhibited a strong frequency dependence over the range 2×10^{-4}–1 Hz, with indications that a relaxation peak was achieved and obeyed time-temperature superposition over this range. The frequency dependence was not that of a simple relaxation process.
(4) The anelastic strain was linear with stress to a first approximation for $T < -30°C$ at all the frequencies examined, and for a frequency of 1 Hz for all the temperatures examined, and was nonlinear elsewhere. Additionally, there were indications that the anelastic strain became nonlinear once a threshold stress was reached under certain experimental conditions.
(5) Below the failure stress, neither the initial direction of loading (tension against compression), nor the number of load cycles had an apparent effect on the anelastic response. There were indications of tension–compression asymmetry in the viscous strain.
(6) Specimens generally failed in tension during the first application of the critical stress level. It was observed in several specimens, however, that failure occurred after several cycles of a critical stress level.
(7) Both the effective elastic and the anelastic properties of the test material were sensitive to microstructural variations. Increased salinity and total porosity caused a decrease in the effective elastic modulus and an increase in the anelastic component of strain

Acknowledgments

The authors express their appreciation to the Ocean Sciences Division and the Solid Mechanics Division of the Office of Naval Research who supported this research. They are also grateful to Derek Yegian and Heather Osgood for the dedicated efforts in preparing specimens and post-test analysis, to Nancy Perron for her many contributions to the specimen growth work, thin-section photography and physical properties determinations, and to Gregory Krajesky for his valuable help in the coldrooms and with data analysis.

References

Anglada, M., and Guiu, F., 1981, *Phil. Mag.* A. **44,** 523–541.
Assur, A., 1958, *Proceedings of the Conference on Arctic Sea Ice*, Easton, Maryland, 24–27 February 1958, National Academy of Sciences, National Research Council Publication No. 598 (Washington, D.C.: National Research Council), pp. 106–138.
Biermann, H., Ungar, T., Pfannenmuller, T., Hoffmann, G., Borbely, A., and Mughrabi, H., 1993, *Acta metall. Mater.*, **41,** 2743–2753.
Bowman, K. J., and Gibala, R., 1992, *Acta metal. mater.*, **40,** 193–200.
Chang, L. N., Taylor, G., and Christian, J. W., 1983, *Acta metall. Mater.*, **31,** 37–42.
Cole, D. M., 1990a, *Cold Regions Science and Technol.*, **18,** 303–321;1990b, *Proceedings of the Ninth International Conference on Offshore Mechanics and Arctic Engineering*,

Houston, TX, 18–23 February, Vol. 4 (New York: American Society of Mechanical Engineers), pp. 265–271; 1991, *Proceedings of the Sixth International Specialty Conference on Cold Regions Engineering*, West Lebanon, New Hampshire, 26–28 February 1991 (New York: American Society of Civil Engineers), pp. 504–518; 1993, *Ice Mechanics–1993, Proceedings of the First Joint Mechanics Meeting of the American Society of Mechanical Engineers, American Society of Civil Engineers and the Society of Engineering Science*, Charlottesville, VA, 6–9 June, Applied Mechanics Division, Vol. 163 (New York: American Society of Mechanical Engineers), pp. 261–272; 1994, *Proceedings of the International Association of Hydraulic Research Twelfth International Ice Symposium*, Vol. 3 (Trondheim, The Norwegian Institute of Technology), pp. 1051–1059; 1995, *Phil. Mag.* A, **72,** 231.

COLE, D. M., and DURELL, G. D., 1995, Cold Regions Research and Engineering Laboratory Report (in press).

COLE, D. M., and GOULD, L. D., 1989, *Proceedings of the Eighth International Conference on Offshore Mechanics and Arctic Engineering*, Vol. IV, edited N. K. Sinha, D. S. Sodhi and J. S. Chung, pp. 37–42; 1990, *Cold Regions Sci. Technol.*, **18,** 295–302.

COLE, D. M., GOULD, L. D., and BURCH, W. B., 1985, *J. Glaciol.*, **31,** 362–365.

COX, G. F. N., and WEEKS, W. F., 1983, *J. Glaciol.*, **29,** 306–316; 1986, *Ibid.*, **32,** 371–375.

DUNAND, D. C., and MORTENSEN, A., 1991, *Acta metall. mater.*, **39,** 127–139.

DUVAL, P., 1978, *J. Glaciol.*, **21,** 621–628.

FUKUDA, A., HONDOH, T., and HIGASHI, A., 1987, *J. Phys., Paris*, **48,** C1-163–C1-173.

GABB, T. P., and WELSCH, G., 1989, *Acta Metall.*, **37,** 2507–2516.

GABORIAUD, R. J., WOIRGARD, J., GERLAND, M., and RIVIERE, A., 1981, *Phil. Mag.* A, **43,** 363–375.

GLADKOV, M. G., NIKITIN, V. A., SMIRNOV, V. N., FEDOROV, B. A., SHUSHLEBIN, A. L., 1983, *Trans. Arctic Antarctic Res. Inst.*, **379,** Translation No. T–833–15.

GOLD, L. W., 1994, *Ann. Glaciol.*, **19,** 13–18.

G'SELL, C., and CHAMPIER, G., 1981, *Phil. Mag.* A, **43,** 1537–1560.

GUPTA, V., PICU, R. C., and FROST, H. J., 1993, *Ice Mechanics 1993*, AMD Vol. 163 (New York: American Society for Mechanical Engineers), pp. 199–216.

HIGASHI, A., 1966, *Proceedings of the International Conference on Low Temperature Science*, (Sapporo: Institute of Low Temperature Science, Hokkaido University), pp. 277–289.

HIKI, Y., and TAMURA, J., 1983, *J. phys. Chem.*, **87,** 4054–4059.

HOBBS, P. V., 1974, *Ice Physics* (Oxford: Clarendon), p. 837.

KRESSEL, H., and BROWN, N., 1967, *Dislocation Dynamics*, edited by A. R. Rosenfield, G. T. Hahn, A. L. Bement and R. L. Jaffee (New York: McGraw-Hill), pp. 337–356.

KUROIWA, D., 1965, Cold Regions Research and Engineering Laboratory Research Report No. 131.

LAKKI, A., SCHALLER, R., NAUER, M., and CARRY, C., 1993, *Acta metall. Mater.*, **41,** 2845–2853.

LANGDON, T. G., and GIFKINS, R. C., 1983, *Acta metall. mater.*, **31,** 927–938.

MAI, C., 1976, *C.r. hebd. Séanc. Acad. Sci., Paris, Sér.* B, **282,** 515–518.

MCKITTRICK, L. R., and BROWN, R. L., 1993, *Ice Mechanics–1993, Proceedings of the First Joint Mechanics Meeting of the American Society of Mechanical Engineers, American Society of Civil Engineers and the Society of Engineering Science*, Charlottesville, VA, 6–9 June, Applied Mechanics Division, Vol. 163 (New York: American Society for Mechanical Engineers), pp. 177–188.

MELLOR, M., and COLE, D. M., 1981, *Cold Regions Sci. Technol.*, **4,** 41–53.

MOTT, N. F., 1957, *Dislocations and Mechanical Properties of Crystals*, edited by J. C. Fisher, W. G. Johnston, R. Thompson and T. Vreeland (New York: Wiley), pp. 458–478.

NAKAMURA, T., and ABE, O., 1979, *J. Fac. Sci., Hokkaido Univ. Ser. VII* (*Geophys.*), **7,** 165–171.

NOWICK A. S., and BERRY, B. S., 1972, *Anelastic Relaxation in Crystalline Solids* (New York: Academic Press), 677pp.

ONSAGER, L., and RUNNELS, L. K., 1969, *J. chem. Phys.*, **50,** 1089–1103.

SHEARWOOD, C., and WHITWORTH, R. W., 1989, *J. Glaciol.*, **35,** 281–283; 1991, *Phil. Mag.* A, **64,** 289–302.

SHIGENAKA, N., MONZEN, R., and MORI, T., 1983, *Acta metall. mater.*, **31,** 2087–2093.

SINHA, N. K., 1979, *Phil. Mag.* A, **40,** 825–842;1990, *Proceedings of the Fourth International Conference on the Creep and Fracture of Engineering Materials and Structures*, University College, Swansea, 1990, Edited by B. Wiltshire and R. W. Evans (London: Institute of Metals), pp. 345–354.

TABATA, T., 1958, *Proceedings of the Conference on Arctic Sea Ice*, Easton, Maryland, 24–27 February 1958, National Academy of Sciences, National Research Council, Publication No. 598 (Washington, D.C.: National Research Council), pp. 139–147.

TABATA, T., and NOHGUCHI, Y., 1979, *Physics and mechanics of Ice*, edited by P. Tryde (New York: Springer), pp. 351–362.

TAKASUGI, T., KISHINO, J., and HANADA, S., 1993, *Acta metall. mater.*, **41,** 1021–1031.

TATIBOUET, J., PEREZ, J., and VASSOILLE, R., 1985, *J. Phys., Paris, Suppl. 12*, **46,** C10–339–C10–342; 1987, *Ibid., Suppl. 3*, **48,** C1–197–C1–203.

TRAETTEBERG, A., GOLD, L. W., and FREDERKING, R., 1975, *Proceedings of the Third International Symposium on Ice Problems*, Hanover, New Hampshire, 1985 (Delft: International Association of Hydraulic Research), pp. 479–486.

TSAI, C. T., YAO, M. W., and CHAIT, A., 1992, *J. Cryst. Growth.*, **125,** 69–80.

VASSOILLE, R., MAI, C., and PEREZ, J., 1978, *J. Glaciol.*, **21,** 375–384.

VAUDREY, K. D., 1977, Naval Civil Engineering Laboratory, Port Hueneme, California, Technical Report No. R860, 81pp.

WEEKS, W. F., and ACKLEY, 1982, *The Growth, Structures, and Properties of Sea Ice*, Cold Regions Research and Engineering Laboratory, Monograph No. 82–1.

WIEDERHORN, S. M., ROBERTS, D. E., CHUANG, T. J., and CHUCK, L., 1988, *J. Am. Ceram. Soc.*, **71,** 602–608.

WOIRGARD, J., RIVIERE, A., and DE FOUQUET, J., 1981, *J. Phys., Paris, Suppl. 10*, **42,** C5–407–C5–419.

ZHAN, C., EVGIN, E., and SINHA, N. K., 1994, *Cold Regions Sci. Technol.*, **22,** 269–284.

ZHU, A. W., and KÊ, T. S., 1989, *Phys. Stat. sol.* (a), **113,** 393–401.